2024 IEEE International Conference on Robotics and Automation (ICRA 2024)
May 13-17, 2024. Yokohama, Japan

Toward a framework integrating augmented reality and virtual fixtures for safer robot-assisted lymphadenectomy

Ziyang Chen[1], Ke Fan[1], Laura Cruciani[1], Matteo Fontana[2], Lorenzo Muraglia[3], Francesco Ceci[3], Laura Travaini[3], Giancarlo Ferrigno[1], *Senior Member, IEEE* and Elena De Momi[1,2], *Senior Member, IEEE*

***Abstract*— Lymphadenectomy generally accompanies various oncology surgeries to remove infected cancer cells. However, there are two limitations in robot-assisted lymphadenectomy: 1) lymph nodes are not visible during operation since they are hidden by the superficial fat layer; 2) intra-operative bleeding may occur during lymph node removal caused by collisions between surgical instruments and delicate blood vessels (arteries or veins) near the lymph nodes. Therefore, we propose a framework integrating augmented reality and virtual fixtures to address these limitations. Augmented reality intra-operatively visualizes the hidden lymph nodes by projecting the corresponding 3D pre-operative model, and virtual fixtures are used to provide force feedback to surgeons to avoid possible collisions when they operate the surgical instruments to resect the lymph nodes surrounding the blood vessel. Ten human subjects were invited to perform an emulated lymphadenectomy based on the da Vinci robot in a dry lab. Experimental results demonstrated that the proposed framework can keep localizing the hidden lymph nodes, and reduce the number of collisions (21% and 48% reduction rates using two different force models compared to the standard setup, respectively) between the instruments and the delicate blood vessel during lymph node resection. It shows the potential to enhance the safety of robot-assisted lymphadenectomy.**

I. INTRODUCTION

Lymphadenectomy is a common surgical procedure that accompanies various tumor surgeries, such as nephrectomy [1], prostatectomy [2], cystectomy [3], and hysterectomy [4]. When cancer cell lesions occur in these areas, there is a possibility of lymph node metastasis, therefore it is necessary to perform lymph node resection in the corresponding area to remove the infected cancer cells. Traditional open or laparoscopic lymphadenectomy has gradually been replaced by Robot-Assisted Lymphadenectomy (RAL) due to the clearer surgical field of view, fewer postoperative complications and recovery time [5]–[7]. Thanks to the success of commerce, Da Vinci Surgical System (DVSS, Intuitive Surgical Inc., US) has been the most popular platform in the operation of RAL as well as other minimally invasive surgeries at the hospital [8], [9]. Nevertheless, there are two challenges when the surgeons control the da Vinci robot to perform the RAL operation. On the one hand, lymph nodes are hidden by the superficial fat layer, making them invisible in the in vivo environment of patients. Surgeons need to use a special probe to search for hidden lymph nodes throughout the whole surgical field following a standard template, which delays the entire surgical process. On the other hand, lymph nodes surround blood vessels (arteries or veins), which increases the risk of damaging blood vessels when lymph nodes are removed. Intra-operative bleeding may occur caused by collisions between surgical instruments and delicate blood vessels when resecting the lymph nodes.

Augmented Reality (AR) provides a promising solution to visualize targets of interest by utilizing information of pre-operative models. Generally, patients are asked to take a Computerized Tomography (CT) or Magnetic Resonance Imaging (MRI) scan for surgeons' surgical planning, and these slices can be processed to obtain the 3D pre-operative model. The pre-operative model is projected onto the intra-operative scenes to provide more visual information, i.e., showing the hidden object by projecting the pre-operative model on the corresponding intra-operative area, and these augmented intra-operative images can guide surgeons to perform surgical procedures. In [10], the authors developed an AR system for the robot-assisted partial nephrectomy. They exploited the CT scans to export a 3D pre-operative model and overlap it on the intra-operative images to show the hilum structure and endophytic tumors. It could show the location of the tumors hidden in the kidney, but it requires an experienced surgeon to manually align the pre-operative model on the intra-operative area. Similarly, the authors in [11], [12] utilized the MRI slices of patients to obtain the 3D anatomical model and visualized it on the intra-operative scenes to guide the surgical dissection by the real-time identification of the index lesion in the robotic radical prostatectomy. Surgical data from the patients showed that the AR technology may improve the surgical outcome, but this approach still relies on the manual registration between the pre-operative model and the intra-operative scenes. To implement the AR assistance in surgery, [13], [14] introduced intra-operative ultrasound to overcome the limitation of manual registration by recovering the depth information of the interested targets although it requires the external probe.

Virtual Fixtures (VFs) are a shared control strategy that ap-

This work involved human subjects in its research. Approval of all ethical and experimental procedures and protocols was granted by the Politecnico di Milano Ethics Committee (Authorization no. 30/2023).

[1]Ziyang Chen, Ke Fan, Laura Cruciani, and Giancarlo Ferrigno are with the Department of Electronics, Information and Bioengineering, Politecnico di Milano, 20133, Italy. ziyang.chen@polimi.it

[2]Matteo Fontana is with the Department of Urology, European Institute of Oncology, IRCCS, Milan, 20141, Italy.

[3]Lorenzo Muraglia, Francesco Ceci, and Laura Travaini are with the Department of Nuclear Medicine, European Institute of Oncology, IRCCS, Milan, 20141, Italy.

[1,2]Elena De Momi is with the Department of Electronics, Information and Bioengineering, Politecnico di Milano, 20133, Italy, and also with the Department of Urology, European Institute of Oncology, IRCCS, Milan, 20141, Italy.

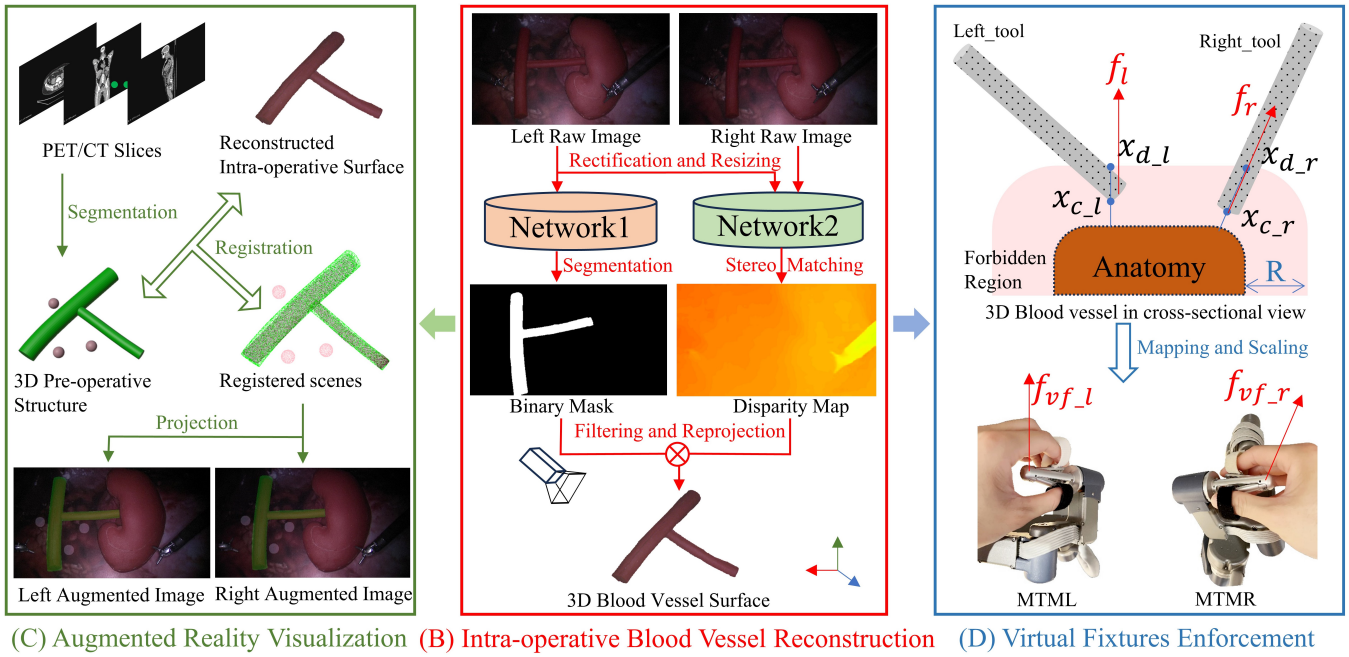

Fig. 1. The proposed framework integrating augmented reality and virtual fixtures. (B) presents the real-time 3D reconstruction of the blood vessel during the operation; (C) shows the visualization of the hidden lymph nodes using the 3D pre-operative model based on augmented reality; (D) demonstrates the enforcement details of virtual fixtures on the manipulators to avoid collisions between the instruments and the delicate blood vessel.

plies computer-generated forces to users as haptic feedback, and they are mainly divided into the guidance VFs (guide users toward a target) and forbidden-region VFs (restrict access to the forbidden region) [15], [16]. It can be seen that forbidden-region VFs have attracted much attention to avoid collision between the instruments and delicate targets in the surgical robot field [17]. By defining a forbidden region near the delicate targets such as the blood vessel, the surgeons will perceive a repulsive force on the manipulators when approaching the defined area to avoid further collisions. The authors in [16] adopted VFs to prevent surgeons from damaging the surface of the heart, and the experimental results showed that it could reduce the error rate with VFs assistance even if the experiment was conducted in a simulator. To avoid collision between two surgical instruments of the da Vinci robot, [18] utilized the VFs technology to force the surgeons to maintain a safe distance when operating the instruments. Although the experiments showed that VFs assistance could help avoid collisions, the experiment was based on a simple custom task. Furthermore, the authors in [19] performed a simple partial nephrectomy with the VFs assistance in a 3D-printed phantom environment. The experiment demonstrated that the VFs assistance can increase the safe distance between the instruments while not introducing delays, but they didn't consider the registration issue so that their method could only work in static scenarios.

Hence, a framework integrating AR and VFs is proposed in this paper to overcome the two limitations of lymphadenectomy for safer operation. Firstly, a markerless AR strategy is conducted to localize the hidden lymph nodes by projecting their 3D pre-operative model onto the intra-operative scenes [20]. Secondly, the VFs strategy is implemented to provide force feedback to surgeons to avoid collisions between the surgical instruments and the delicate blood vessel when the surgeons operate the da Vinci robot to resect the surrounding lymph nodes. The framework has high generalization in other surgical applications since it does not rely on specific devices and platforms. Finally, a usability study involving ten participants is conducted to explore the feasibility of the proposed framework by performing a lymphadenectomy on a phantom.

II. METHODOLOGY

Fig. 1 shows the framework architecture integrating AR and VFs. It was integrated into the da Vinci Research Kit (dVRK) in Leonardo Robotics Lab, Politecnico di Milano, Italy. Intra-operative blood vessel reconstruction is a prerequisite of AR and VFs, which recovers 3D intra-operative position information of the blood vessel in real time. Then, the 3D pre-operative model is transformed to the corresponding intra-operative position through registration with the reconstructed blood vessel, and AR is exploited to visualize the hidden lymph nodes. Finally, VFs are adopted for collision avoidance between the surgical instruments and the delicate blood vessel when resecting the lymph nodes. The specific framework description is as follows.

A. DVRK robot

DVRK robot (Intuitive Surgical Inc., US, and Johns Hopkins University) is the most popular surgical research platform which consists of the leader side and the follower side. Surgeons can control the two Master Tool Manipulators (MTMs) to tele-operate the robot and observe the surgical

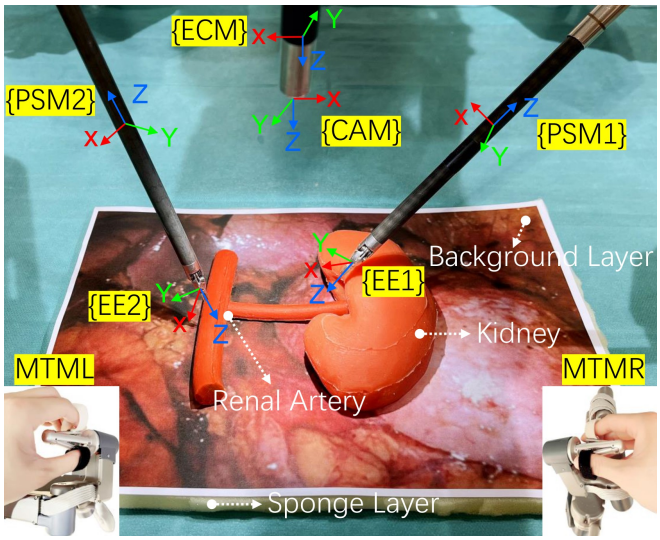

Fig. 2. The dVRK experimental platform and the definition of reference frames. "MTML" and "MTMR" are the left and right manipulators handled by surgeons to remotely control the movement of surgical instruments. It also demonstrates a phantom for emulating the lymphadenectomy, where lymph nodes are hidden in a sponge layer beneath the background layer.

scenes using the High-Resolution Stereo Viewer (HRSV) at the leader side. On the other side, the surgical instruments mounted on the two Patient Side Manipulators (PSMs) move following the surgeons' hands, and the stereo endoscope mounted on the Endoscope Camera Manipulator (ECM) keeps recording the stereo scenes during operation. The reference frames of the dVRK robot are shown in Fig. 2, and the base frame we defined is $\{ECM\}$. Three types of calibrations are performed to run the framework and find out the unknown transformation matrices between different frames, including camera calibration, hand-eye calibration and hand-hand calibration. Zhang's method [21] is conducted to generate the intrinsic and extrinsic camera parameters by using a 9×6 chessboard. The hand-eye transformation matrix T_{ECM}^{CAM} is generated based on the RANSAC method [22], [23] by controlling the end effector of the left instrument pointing at all chessboard corners. Finally, the hand-hand transformation matrix T_{EE1}^{EE2} is achieved based on the Horn's method [24] by moving the two instruments pointing at 40 non-linear points.

B. Intra-operative blood vessel reconstruction

Lymph nodes are invisible during operation since they are always hidden in the fat layer, however, the blood vessel surrounding lymph nodes is visible since it is exposed on the surface of soft tissues. It provides the possibility to localize the lymph nodes by referencing the blood vessel since the relative position between the blood vessel and the lymph nodes is fixed and it can be obtained based on their pre-operative model. As long as pre-operative lymph nodes are transformed to the correct intra-operative positions, AR can be used to visualize them on intra-operative images. On the other hand, the VFs enforcement requires the distance between the blood vessel and the surgical instruments. The position of instruments can be subscribed from the dVRK kinematics, but the position of the blood vessel remains unknown. Hence, intra-operative blood vessel reconstruction is the foundation for implementing AR and VFs. The dVRK endoscope captures stereo images with a resolution of 1920×1080, and the images are resized to 640×360 to accelerate the framework and rectified to align the horizontal epipolar line. Then, a disparity estimation-based stereo matching network [25] is adopted to perform the surgical scene reconstruction since it provides a fast and accurate reconstruction effect. Another segmentation network is required to extract the region of interest (i.e., the blood vessel) from the estimated disparity map for the accurate registration purpose, and UNet [26] is selected as the segmentation model since it provides a stable segmentation quality in our experiment. The weight of the UNet model is trained from the scratch using 551 manually annotated images captured from the dVRK endoscope. Finally, we can reproject the disparity map of the blood vessel into the 3D space to reconstruct the intra-operative blood vessel as a point cloud.

C. Augmented reality visualization

A 3D pre-operative model is obtained by CT or MRI slices, and it provides the space position of organs and soft tissues even if these objects are invisible in the intra-operative phase. In our case, we use a 3D modeling software (Blender) to generate the 3D pre-operative model including the blood vessel and lymph nodes for simplification. After reconstructing the intra-operative blood vessel, we perform the registration between the pre-operative and intra-operative blood vessels so that the lymph nodes can be transformed to the corresponding intra-operative position. The global registration-based RANSAC algorithm [22] is performed once at the initial position, and the local registration-based ICP algorithm [27] is adopted to finetune the position of the pre-operative model, which produces a satisfactory registration result in both speed and accuracy from our observation. After registration, the pre-operative model is projected on the 2D intra-operative images based on the hand-eye transformation so that the lymph nodes can be visible on the augmented intra-operative scenes. In this way, the surgeons can be guided to localize the lymph nodes when observing the endoscopic scenes.

D. VFs enforcement

Surgical instruments may collide with the surrounding blood vessel during lymph node removal, resulting in intra-operative bleeding. To solve this issue, VFs are adopted to generate a repulsive force $\vec{F}$ to prevent possible collisions when surgeons operate the surgical instruments to approach the delicate anatomy (blood vessel in our case) in the defined forbidden region, and the force is calculated based on the distance between the instruments and the blood vessel. The 3D intra-operative position of the blood vessel is recovered using the stereo reconstruction and segmentation, and the 3D positions of surgical instruments including the origins of $\{PSM1\}$, $\{PSM2\}$, $\{EE1\}$ and $\{EE2\}$ shown in Fig. 2 are

TABLE I

THE COMPUTATIONAL TIME DISTRIBUTION OF THE FRAMEWORK

Component	Time (ms)
Intra-operative blood vessel reconstruction	95.0±3.7
Augmented reality visualization	24.4±3.5
Virtual fixtures enforcement	13.4±1.7
Whole framework	135.5±7.7

subscribed from the direct kinematics and modeled as point clouds so that the minimum distance can be calculated using the fast k-nearest-neighbor search algorithm [28], [29]. Then, two models with different trends in force and distance are proposed to calculate the VFs force,

1) Generalized sigmoid force [16]: The force $\overrightarrow{F_{gs}}$ is proportional to the minimum distance x_c within the forbidden region,

$$\overrightarrow{F_{gs}} = \begin{cases} \left(\frac{2}{1+e^{-k_{gs}(x_c - R/2)}} + 1\right)\vec{n} & \text{if } x_c \leq R \\ 0 & \text{if } x_c > R \end{cases} \quad (1)$$

where k_{gs} is the constant factor to control the curvature degree of the generated force curve, and R is the range of the forbidden region surrounding the anatomical surface. $\vec{n}$ is the direction vector of the VFs force, and its orientation is defined as the outward direction from the minimum distance point on the anatomy surface to the corresponding point of the surgical instrument.

2) Visco-elastic force [18]: The force $\overrightarrow{F_{ve}}$ and the distance x_c are inversely proportional within the forbidden region,

$$\overrightarrow{F_{ve}} = \begin{cases} k_{ve}\left(x_d - x_c\right)\vec{n} + b_{ve}\left(\dot{x}_d - \dot{x}_c\right)\vec{n} & \text{if } x_c \leq R \\ 0 & \text{if } x_c > R \end{cases} \quad (2)$$

where x_d is the desired minimum distance between the instrument and the delicate anatomy while x_c is the current minimum distance. $\dot{x}_d$ and $\dot{x}_c$ are their derivatives, respectively. k_{ve} and b_{ve} are the elastic and dumping constants. Finally, the calculated VFs forces are mapped on the MTMs based on a closed-loop impedance controller [18], and the users can feel force feedback when operating the instruments in the forbidden region.

III. EXPERIMENT AND RESULTS

A. Framework quantitative evaluation

1) Computational time measurement: The computational time of the whole framework was recorded based on 100 frames of dynamic scenes, and the computing resource is an Nvidia 3080 GPU. The specific time distribution is shown in Table I. Part (B) Intra-operative blood vessel reconstruction takes the most time in this framework since it contains the inference of two neural networks (the time of stereo matching model [25] is 36.9±1.8ms, and the segmentation model [26] takes 42.5±0.8ms), while VFs enforcement takes the minimum time. The whole framework takes around 0.1355s per frame, which can provide smooth feedback to the users when operating the robot.

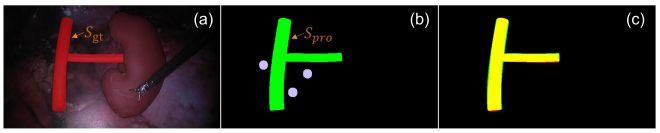

Fig. 3. Scheme to evaluate the registration accuracy for augmented reality. (a) is the intra-operative image with the manually annotated ground truth of the blood vessel; (b) is the 2D projection of the pre-operative model (the green object is the blood vessel while the pink circles represent the lymph nodes); (C) overlays the projection of pre-operative blood vessel (green color) onto the ground truth of intra-operative blood vessel (red color), and the yellow area is their coverage.

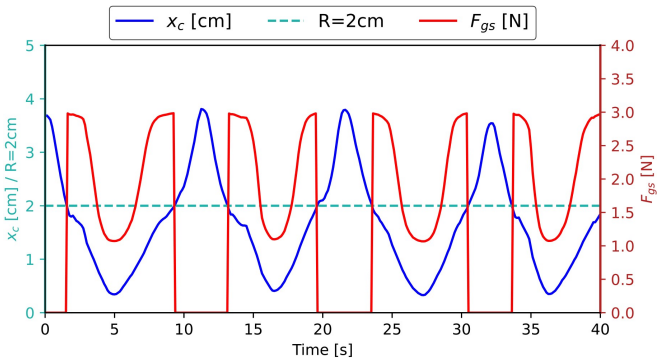

Fig. 4. The distance and force norm data based on the generalized sigmoid model. The threshold of the forbidden region is set to 2cm.

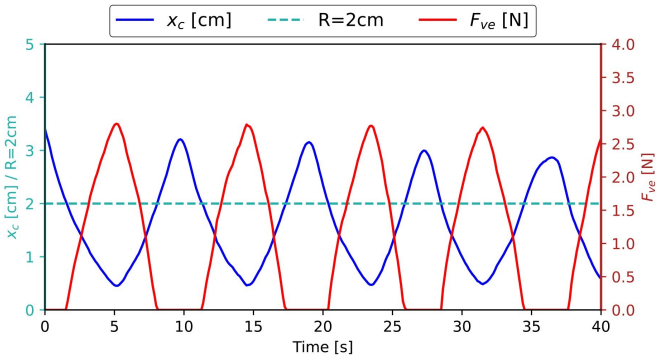

Fig. 5. The distance and force norm data using the visco-elastic model.

2) Augmented reality performance: To evaluate the accuracy of augmented reality, we considered calculating the Dice similarity coefficient by comparing the projected pre-operative blood vessel with the manually annotated intra-operative blood vessel [30],

$$\text{Dice}(S_{pro}, S_{gt}) = \frac{2|S_{pro} \cap S_{gt}|}{|S_{pro}| + |S_{gt}|} \quad (3)$$

where S_{pro} is the projected area of the pre-operative blood vessel, while S_{gt} is the area of the intra-operative blood vessel using the manual annotation. Fig. 3 demonstrates the schematic diagram of the evaluation metric. 100 dynamic image sets (including both the projected pre-operative blood vessel and the intra-operative blood vessel) were captured, and the final Dice value is 0.9293±0.0091, which reflects that the pre-operative model can accurately track the corresponding intra-operative target.

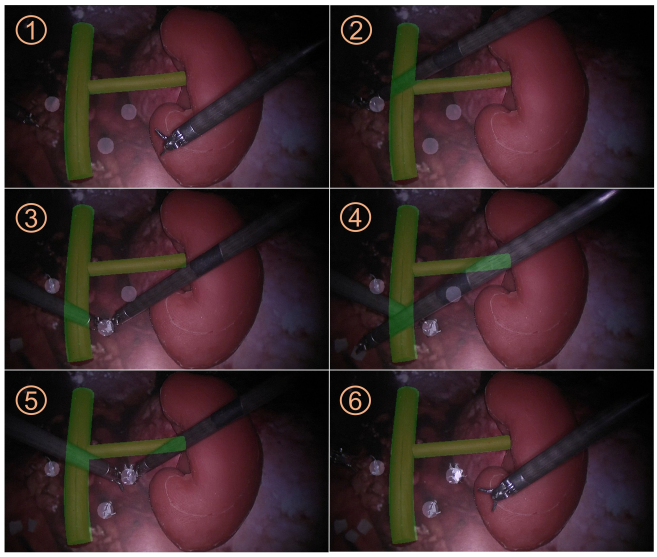

Fig. 6. The demonstration of the emulated robot-assisted lymphadenectomy in a dry lab. The three pink circles present the location of the lymph nodes hidden under the background layer using AR. Frame 1 shows the initial position of the task. In Frame 2, the user operates the surgical instruments to cut the background layer and clamp the lymph node (white small object) hidden in the sponge layer, and move the lymph node to the bottom left corner as shown in Frame 3. Then, the user performs the same operation to resect the other two lymph nodes (i.e., cut the background layer, clamp the white objects from the sponge layer and move them to the bottom left corner) as shown in Frame 3 to 5. Finally, the user moves the instruments to the same position as the initial one in Frame 6.

3) Virtual fixtures performance: Two force models with opposite proportional relationships to distance were introduced for collision avoidance. In the generalized sigmoid force model, the constant factor k_{gs} is set to 500, and the threshold R is set to 2cm. In the visco-elasitic force model, k_{ve}=180 N/m and b_{ve}=9 N·s/m. x_d is set to be equal to R, while $\dot{x}_d$ is 0. The maximum force norm is 3N in both the generalized sigmoid model and the visco-elastic model. To verify the VFs performance, the surgical instruments were moved regularly at the boundary of the forbidden region, and the minimum distance and estimated force norm curves of the two models are given in Fig. 4 and Fig. 5, respectively. It shows that the VFs force can be accurately estimated following the minimum distance variation.

B. Framework usability study

To evaluate the usability of the proposed framework, a robot-assisted lymphadenectomy was emulated in a phantom environment based on the dVRK platform, as shown in Fig. 2. The 3D-printed blood vessel (renal artery) and kidney were visible during the operation, and the three lymph nodes were hidden under the background layer to simulate the abdominal environment. Here, we used a layer of sponge to pad under the background and the lymph nodes were inside the sponge to simulate the real situation where the lymph nodes are located in the superficial fat layer. Hence, AR was adopted to visualize the three lymph nodes hidden in the sponge layer beneath the background, and VFs were exploited to provide haptic feedback to users when the surgical instruments approach the blood vessel in the forbidden region during lymph node removal.

Ten human subjects (non-specialists) aged between 21 and 28 were invited to operate the emulated lymphadenectomy, and the defined task was to teleoperate the surgical instruments to cut the background layer, clamp the lymph nodes (white small objects) hidden in the sponge covered by the background layer and move them to the bottom left corner of the intra-operative field, as shown in Fig. 6. Three different VFs modalities were compared to perform the defined task,

- C: The users don't receive force feedback when the instruments approach the blood vessel in the forbidden region;
- F_{gs} 1: The users perceive a repulsive force calculated by the generalized sigmoid model in the forbidden region (the force decreases when the minimum distance between the instrument and the delicate blood vessel decreases);
- F_{ve} 2: The users receive a repulsive force calculated by the visco-elastic model when working in the forbidden region (the force increases when the minimum distance decreases).

Before the experiment, the users were provided 15 minutes to become familiar with the dVRK platform as well as its operation. The tasks were performed for three rounds, and the three VFs modalities were performed randomly in each round. The third-round data was utilized for the result analysis to avoid the potential impact of the learning curve. Four performance metrics were adopted to evaluate the feasibility of the VFs assistance, including (a) the average value of the distance D_{mean} when surgical instruments work in the forbidden region of 2cm,

$$D_{\text{mean}} = \frac{1}{m+n}\left(\sum_{i=1}^{m} x_{cL}^{i} + \sum_{j=1}^{n} x_{cR}^{j}\right) \tag{4}$$

where x_{cL}^{i} and x_{cR}^{j} are the i-th and k-th minimum distance points of the left and right instruments within the forbidden region of 2cm, respectively. m and n are the number of the minimum distance points of the left and right instruments in the forbidden region. (b) The minimum value of the distance D_{min} when working in the forbidden region, and it is the minimum value of the set $\{x_{cL}^{1}, \ldots, x_{cL}^{m}, x_{cR}^{1}, \ldots, x_{cR}^{n}\}$. (c) The collision number N_c when the distance between the instrument and the delicate blood vessel is less than r_{c} in one second, we regard it as one time of collision,

$$N_{\text{c}} = \sum_{i=1}^{m}\left\{1 \mid x_{cL}^{i} < r_{\text{c}}\right\} + \sum_{j=1}^{n}\left\{1 \mid x_{cR}^{j} < r_{\text{c}}\right\} \tag{5}$$

where r_{c} is the threshold to be regarded as a collision and it is set to 0.5cm. (d) The execution time T_{exe} to perform the whole task. The Wilcoxon signed-rank test ($p < 0.05$) was introduced to explore if there were significant differences among the three different VFs modalities [31]. After the experiment, the users filled out the NASA-TLX questionnaire by giving a score from 0 to 100 based on six questions, to evaluate if the VFs assistance will introduce extra load in six aspects including mental demand, physical demand, temporal demand, performance, effort and frustration [32].

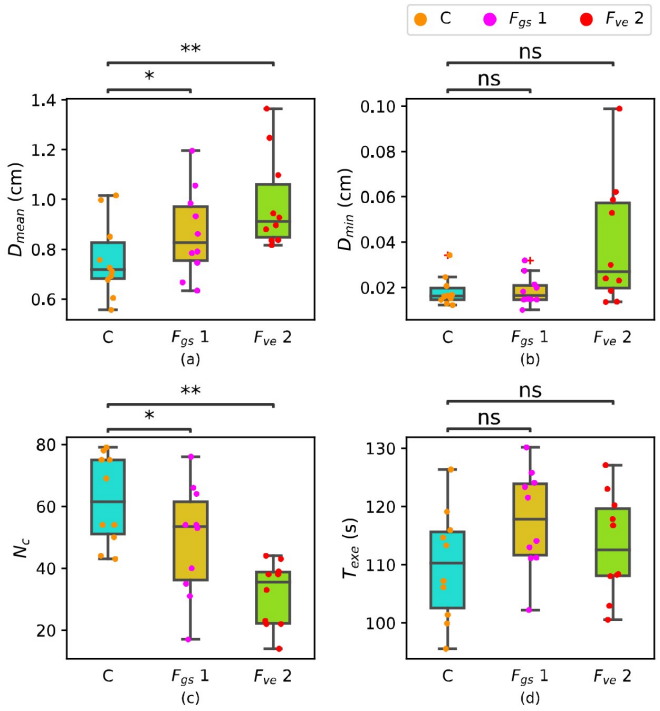

Fig. 7. The data captured from ten human subjects. "C" means that there is no VFs assistance, "F_{gs}" means that the VFs force is generated based on the generalized sigmoid model, while "F_{ve}" is with the VFs force calculated by the visco-elastic model. The statistical result based on the Wilcoxon signed-rank test is shown as $ns : 0.05 < p \leq 1$, $* : 0.01 < p \leq 0.05$, $** : 0.001 < p \leq 0.01$, and $*** : p \leq 0.001$.

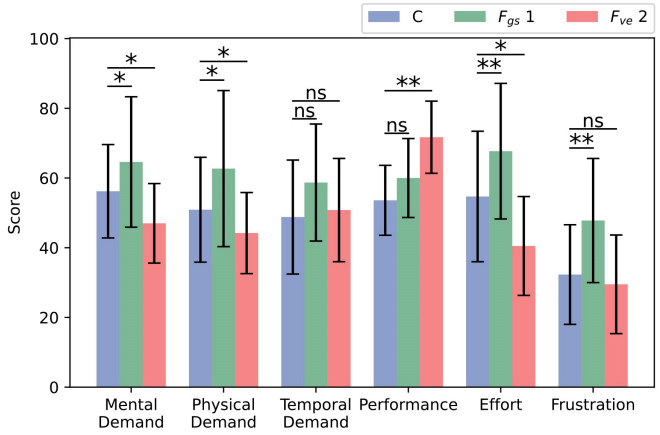

Fig. 8. The scores provided by ten human subjects based on the NASA-TLX questionnaire.

Fig. 7 presents the quantitative result of the usability study based on the ten users. The statistical results show that the mean distance D_{mean} significantly increases with the VFs assistance (the average value of C group is 0.76cm, F_{gs} 1 group is 0.87cm, and F_{ve} 2 group is 0.98cm), and the collision number N_{c} significantly reduces (the average values are C: 62, F_{gs} 1: 49, and F_{ve} 2: 32, respectively), which indicate that the VFs assistance increases the surgical safety (i.e., reduce the possibility of intra-operative bleeding). Also, the visco-elastic model can obtain better performance compared to the generalized sigmoid model. Moreover, the minimum distance D_{min} does not have significant differences in the three modalities, since we noticed that when users cut the background layer, surgical instruments inevitably move towards the blood vessel. Finally, there is no significant difference when referencing the execution time T_{exe}, which shows that the VFs assistance does not introduce the extra temporal load. Fig. 8 shows the result of the NASA-TLX questionnaire. The generalized sigmoid model brings higher mental and physical load compared to the standard setup, since it suddenly applies a strong force when entering the boundary of the forbidden region which requires more effort to control surgical instruments according to the feedback of users. As a comparison, the users prefer the force generated by the visco-elastic model because of its progressive mode.

IV. DISCUSSION AND CONCLUSION

AR has been gradually introduced in robotic surgery since it provides the possibility to show the invisible organs or soft tissues in intra-operative scenes by utilizing the information of the corresponding pre-operative model. To overcome the limitation of lymph node localization, i.e., surgeons need to use a probe to localize lymph nodes hidden in the superficial fat layer and this process is often time-consuming, we introduced AR to localize the lymph nodes by referencing the blood vessel near them since the blood vessel is generally exposed. The experimental result based on the phantom environment shows that the pre-operative model can keep tracking the intra-operative blood vessel so that the lymph nodes can be accurately localized during the operation. On the other hand, intra-operative bleeding is a dangerous situation caused by collisions between surgical instruments and delicate blood vessels, e.g., it is possible to damage the blood vessel when performing the lymph node resection since the lymph nodes always surround the blood vessel, so VFs are adopted to avoid the possible collisions. The result in Fig. 7 shows that the introduction of VFs can significantly increase the safe distance and reduce the collision number while not introducing the extra operation duration. From the feedback of the users, the visco-elastic force can provide a more comfortable experience compared to the generalized sigmoid force since they prefer that the force increases when the distance decreases.

To sum up, an AR and VFs-based framework is proposed to visualize the hidden lymph nodes and avoid collisions between the surgical instruments and the delicate blood vessel near the lymph nodes, which aims to enhance the safety of RAL operation. The quantitative evaluation shows that our framework can accurately and fastly perform the AR visualization and the VFs enforcement. Also, the usability study based on ten human subjects indicates that the force feedback generated by the VFs assistance has the potential to enhance surgical safety by avoiding collisions with delicate blood vessels. In the future, this framework will be applied to a hospital (European Institute of Oncology, Milan, Italy) to verify its practicality in robot-assisted lymphadenectomy.

REFERENCES

[1] P. A. Hargis, B. Henslee, N. Pokala, and A. Bhat, "Percutaneous lymphatic maceration and glue embolization for high-output chylous ascites after robot-assisted laparoscopic nephrectomy and lymphadenectomy," *Journal of Clinical Imaging Science*, vol. 11, 2021.

[2] V. Student Jr, Z. Tudos, Z. Studentova, O. Cesak, H. Studentova, V. Repa, D. Purova, and V. Student, "Effect of peritoneal fixation (perfix) on lymphocele formation in robot-assisted radical prostatectomy with pelvic lymphadenectomy: Results of a randomized prospective trial," *European Urology*, vol. 83, no. 2, pp. 154–162, 2023.

[3] K. S. Faraj, H. M. Abdul-Muhsin, K. M. Rose, A. K. Navaratnam, M. W. Patton, S. Eversman, R. Singh, W. G. Eversman, S. M. Cheney, M. D. Tyson *et al.*, "Robot assisted radical cystectomy vs open radical cystectomy: over 10 years of the mayo clinic experience," in *Urologic Oncology: Seminars and Original Investigations*, vol. 37, no. 12. Elsevier, 2019, pp. 862–869.

[4] B. Chen, M. Ji, P. Li, P. Liu, W. Zou, Z. Zhao, B. Qu, Z. Li, X. Bin, J. Lang *et al.*, "Comparison between robot-assisted radical hysterectomy and abdominal radical hysterectomy for cervical cancer: a multicentre retrospective study," *Gynecologic oncology*, vol. 157, no. 2, pp. 429–436, 2020.

[5] G. J. Rodrigues, G. B. Guglielmetti, M. Orvieto, K. R. S. Bhat, V. R. Patel, and R. F. Coelho, "Robot-assisted retroperitoneal lymphadenectomy: The state of art," *Asian Journal of Urology*, vol. 8, no. 1, pp. 27–37, 2021.

[6] H. Yu, Y. Lu, Y. Xiao, J. Guo, X. Yin, Y. Yang, H. Wang, and J. Gao, "Robot-assisted laparoscopic antegrade versus open inguinal lymphadenectomy: a retrospective controlled study," *BMC urology*, vol. 19, pp. 1–7, 2019.

[7] Z. Chen, A. Marzullo, D. Alberti, E. Lievore, M. Fontana, O. De Cobelli, G. Musi, G. Ferrigno, and E. De Momi, "Frsr: Framework for real-time scene reconstruction in robot-assisted minimally invasive surgery," *Computers in Biology and Medicine*, p. 107121, 2023.

[8] E. Bentivegna, M. Koual, H.-T. Nguyen-Xuan, L. Plait, S. Seidler, G. Achen, A.-S. Bats, and H. Azaïs, "Docking for robotic extraperitoneal para-aortic lymphadenectomy with da vinci xi surgical system," *Journal of Gynecology Obstetrics and Human Reproduction*, vol. 50, no. 8, p. 102131, 2021.

[9] Z. Chen, S. Terlizzi, T. Da Col, A. Marzullo, M. Catellani, G. Ferrigno, and E. De Momi, "Robot-assisted ex vivo neobladder reconstruction: preliminary results of surgical skill evaluation," *International Journal of Computer Assisted Radiology and Surgery*, vol. 17, no. 12, pp. 2315–2323, 2022.

[10] A. Hamada, A. Sawada, J. Kono, M. Koeda, K. Onishi, T. Kobayashi, T. Yamasaki, T. Inoue, H. Noborio, and O. Ogawa, "The current status and challenges in augmented-reality navigation system for robot-assisted laparoscopic partial nephrectomy," in *Human-Computer Interaction. Multimodal and Natural Interaction: Thematic Area, HCI 2020, Held as Part of the 22nd International Conference, HCII 2020, Copenhagen, Denmark, July 19–24, 2020, Proceedings, Part II 22*. Springer, 2020, pp. 620–629.

[11] L. Bianchi, F. Chessa, A. Angiolini, L. Cercenelli, S. Lodi, B. Bortolani, E. Molinaroli, C. Casablanca, M. Droghetti, C. Gaudiano *et al.*, "The use of augmented reality to guide the intraoperative frozen section during robot-assisted radical prostatectomy," *European Urology*, vol. 80, no. 4, pp. 480–488, 2021.

[12] R. Schiavina, L. Bianchi, S. Lodi, L. Cercenelli, F. Chessa, B. Bortolani, C. Gaudiano, C. Casablanca, M. Droghetti, A. Porreca *et al.*, "Real-time augmented reality three-dimensional guided robotic radical prostatectomy: preliminary experience and evaluation of the impact on surgical planning," *European Urology Focus*, vol. 7, no. 6, pp. 1260–1267, 2021.

[13] T. Wendler, F. W. van Leeuwen, N. Navab, and M. N. van Oosterom, "How molecular imaging will enable robotic precision surgery: The role of artificial intelligence, augmented reality, and navigation," *European Journal of Nuclear Medicine and Molecular Imaging*, vol. 48, no. 13, pp. 4201–4224, 2021.

[14] G. Samei, K. Tsang, C. Kesch, J. Lobo, S. Hor, O. Mohareri, S. Chang, S. L. Goldenberg, P. C. Black, and S. Salcudean, "A partial augmented reality system with live ultrasound and registered preoperative mri for guiding robot-assisted radical prostatectomy," *Medical image analysis*, vol. 60, p. 101588, 2020.

[15] D. Bazzi, F. Roveda, A. M. Zanchettin, and P. Rocco, "A unified approach for virtual fixtures and goal-driven variable admittance control in manual guidance applications," *IEEE Robotics and Automation Letters*, vol. 6, no. 4, pp. 6378–6385, 2021.

[16] J. Ren, R. V. Patel, K. A. McIsaac, G. Guiraudon, and T. M. Peters, "Dynamic 3-d virtual fixtures for minimally invasive beating heart procedures," *IEEE transactions on medical imaging*, vol. 27, no. 8, pp. 1061–1070, 2008.

[17] A. Venugopal, S. Moccia, S. Foti, A. Routray, R. A. MacLachlan, A. Perin, L. S. Mattos, A. K. Yu, J. Leonardo, E. De Momi *et al.*, "Real-time vessel segmentation and reconstruction for virtual fixtures for an active handheld microneurosurgical instrument," *International Journal of Computer Assisted Radiology and Surgery*, vol. 17, no. 6, pp. 1069–1077, 2022.

[18] R. Moccia, C. Iacono, B. Siciliano, and F. Ficuciello, "Vision-based dynamic virtual fixtures for tools collision avoidance in robotic surgery," *IEEE Robotics and Automation Letters*, vol. 5, no. 2, pp. 1650–1655, 2020.

[19] A. Banach, K. Leibrandt, M. Grammatikopoulou, and G.-Z. Yang, "Active contraints for tool-shaft collision avoidance in minimally invasive surgery," in *2019 International Conference on Robotics and Automation (ICRA)*. IEEE, 2019, pp. 1556–1562.

[20] Z. Chen, L. Cruciani, K. Fan, M. Fontana, E. Lievore, O. D. Cobelli, G. Musi, G. Ferrigno, and E. D. Momi, "Towards safer robot-assisted surgery: A markerless augmented reality framework," *arXiv preprint arXiv:2309.07693*, 2023.

[21] Z. Zhang, "A flexible new technique for camera calibration," *IEEE Transactions on pattern analysis and machine intelligence*, vol. 22, no. 11, pp. 1330–1334, 2000.

[22] M. A. Fischler and R. C. Bolles, "Random sample consensus: a paradigm for model fitting with applications to image analysis and automated cartography," *Communications of the ACM*, vol. 24, no. 6, pp. 381–395, 1981.

[23] B. Sekachev, N. Manovich, M. Zhiltsov, A. Zhavoronkov, D. Kalinin, B. Hoff, D. Kruchinin, A. Zankevich, and D. Sidnev, "opencv/cvat: v1. 1.0," *Zenodo*, 2020.

[24] B. K. Horn, "Closed-form solution of absolute orientation using unit quaternions," *Josa a*, vol. 4, no. 4, pp. 629–642, 1987.

[25] G. Yang, J. Manela, M. Happold, and D. Ramanan, "Hierarchical deep stereo matching on high-resolution images," in *Proceedings of the IEEE/CVF Conference on Computer Vision and Pattern Recognition*, 2019, pp. 5515–5524.

[26] O. Ronneberger, P. Fischer, and T. Brox, "U-net: Convolutional networks for biomedical image segmentation," in *Medical Image Computing and Computer-Assisted Intervention–MICCAI 2015: 18th International Conference, Munich, Germany, October 5-9, 2015, Proceedings, Part III 18*. Springer, 2015, pp. 234–241.

[27] P. J. Besl and N. D. McKay, "Method for registration of 3-d shapes," in *Sensor fusion IV: control paradigms and data structures*, vol. 1611. Spie, 1992, pp. 586–606.

[28] F. Williams, "Point cloud utils," 2022, https://www.github.com/fwilliams/point-cloud-utils.

[29] V. Garcia, E. Debreuve, and M. Barlaud, "Fast k nearest neighbor search using gpu," in *2008 IEEE Computer Society Conference on Computer Vision and Pattern Recognition Workshops*. IEEE, 2008, pp. 1–6.

[30] V. Penza, E. De Momi, N. Enayati, T. Chupin, J. Ortiz, and L. S. Mattos, "Envisors: Enhanced vision system for robotic surgery. a user-defined safety volume tracking to minimize the risk of intraoperative bleeding," *Frontiers in Robotics and AI*, vol. 4, p. 15, 2017.

[31] S. Macciò, A. Carfì, and F. Mastrogiovanni, "Mixed reality as communication medium for human-robot collaboration," in *2022 International Conference on Robotics and Automation (ICRA)*. IEEE, 2022, pp. 2796–2802.

[32] S. G. Hart, "Nasa-task load index (nasa-tlx); 20 years later," in *Proceedings of the human factors and ergonomics society annual meeting*, vol. 50, no. 9. Sage publications Sage CA: Los Angeles, CA, 2006, pp. 904–908.